Optics Communications 475 (2020) 126207

Contents lists available at ScienceDirect

Optics Communications

journal homepage: www.elsevier.com/locate/optcom

Silica based biocompatible random lasers implantable in the skin

Van Duong Ta [a,*], Tam Trong Nguyen [b], Thi Ha Lien Nghiem [c], Hong Nhung Tran [c], Anh Tu Le [d], Nguyen Thuan Dao [d], Phuoc Dinh Duong [a], Hanh Hong Mai [b]

[a] Department of Optical Devices, Le Quy Don Technical University, Hanoi 100000, Viet Nam
[b] Department of Quantum Optics, Faculty of Physics, University of Science, Vietnam National University, Hanoi 100000, Viet Nam
[c] Institute of Physics, Vietnam Academy of Science and Technology (VAST), Hanoi 100000, Viet Nam
[d] Institute of Materials Science, Vietnam Academy of Science and Technology (VAST), Hanoi 100000, Viet Nam

ARTICLE INFO

Keywords:
Random laser
Silica nanoparticle
Biocompatible
Implantable
Skin

ABSTRACT

We demonstrate efficient random lasing from microslices containing dye-doped colloidal silica nanoparticles. The nanoparticles with diameters of 20 nm were synthesized by a modified Stöber method, having a high emission efficiency and well dispersed in an aqueous medium. From the suspension of the nanoparticles, a film is created via self-assembly of colloidal nanoparticles. After grinding the film, microslices with dimensions of around 100–200 μm and thickness of 2 μm are obtained. Under optical pulse excitation, these microslices emit random lasing. The lasers operate well in the air and also in water. Their emission spectrum and lasing threshold in both conditions are studied and compared. Interestingly, lasing emission can be observed from a laser embedded into the porcine skin tissue. Our work provides a simple technique and architecture for biocompatible random lasers which have potential for biosensing and biological probes.

1. Introduction

Random lasers have attracted a great deal of research interest due to their simple and cost-effective fabrication [1]. This kind of laser offers rich physical properties and holds great potential for cost-effective light sources, speckle-free laser imaging, remote sensing and medical diagnostics [2,3]. Random lasers are different from conventional lasers, they do not rely on a proper cavity but on a highly scattering medium to trap and amplify light. As a result, colloidal based systems, which usually provide strong light scattering, are appropriate for the generation of random lasing. Indeed, one of the first random lasers was observed from colloidal suspensions [4]. Later works demonstrate random lasing from other colloidal structures such as semiconductor powders [5], photonic glasses [6], and colloidal quantum dots [7].

Fluorescent colloidal silica nanoparticles (SNPs), owing to biocompatibility and stability in an adverse environment, have been widely used for biomarker, diagnostics and therapeutic applications in cancer diagnosis and drug delivery [8–11]. Despite these advantages, SNPs had not employed for lasers until 2008 when García-Revilla et al. demonstrated random lasing from dye-doped silica gel powder [12]. In this work, silica gel was needed for serving as a matrix material. Recently, random lasing was observed from dye-doped silica powder without using silica gel [13]. However, random lasing from a silica-based microslice structure and the ability to make it lase in an aqueous and biological medium have not been explored.

In this work, we demonstrate random lasing from solid microslices containing dye-doped SNPs fabricated by self-assembly technique. This kind of random laser, which we call microslice lasers, can operate well in various media including in the air, water and skin tissue.

2. Experimental methods

2.1. Fabrication of dye-doped silica nanoparticles

Rhodamine B (RhB)-doped silica nanoparticles (SNPs) were synthesized by a modified Stöber method from methyltrimethoxysilane (MTEOS) and aminopropyl triethoxysilane (APTEOS) precursors. The fabrication process was described in the previous work [10]. Briefly, the micelles were prepared by dissolving 0.22 g aerosol orange T and 400 μL 2-butanone (11 M) in 20 ml of double distilled water by vigorous magnetic stirring. Then, 100 μL RhB in dimethylsulfoxide (10 mM) was added in the micelle solution. After that, 200 μL of MTEOS was added to the micellar system and 40 μL of APTEOS was added 30 min later. Consequently, RhB-doped SNPs were formed. The solution was continuously stirred for 20 h at room temperature for good dispersion. All the surfactant and the remaining chemical agents were removed by dialysing in a 10 kDa molecular-weight cut off (MWCO) dialysis tubing against water for a week.

* Corresponding author.
E-mail address: duong.ta@mta.edu.vn (V.D. Ta).

https://doi.org/10.1016/j.optcom.2020.126207
Received 13 April 2020; Received in revised form 18 June 2020; Accepted 19 June 2020
Available online 22 June 2020

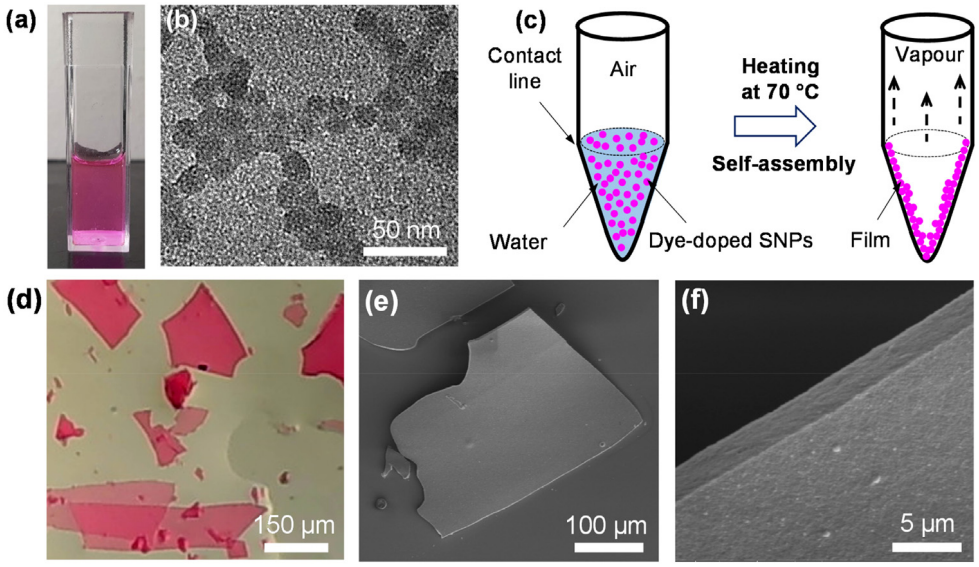

Fig. 1. (a) Optical image of dye-doped SNPs dispersed in water. (b) Transmission electron microscopy (TEM) image of the dye-doped SNPs indicates the particle size of around 20 nm. (c) Schematic of self-assembled process of the colloidal SNPs. (d) and (e) Optical microscope and SEM image of dye-doped SNP microslices. (f) High-magnification SEM image of an edge of a typical microslice indicating a thickness of around 2 μm.

2.2. Optical characterizations

RhB-doped SNP microslices were characterized by using a micro-photoluminescence (μ-PL) setup. The pumping source was a pulsed green laser (Nd:YAG, Litron Lasers) with a wavelength of 532 nm, a repetition rate of 10 Hz and a pulse duration of 7 ns. The exciting laser beam was guided to the film and subsequently focused on the sample with a beam spot diameter of about 350 μm. Emission from the sample was collected by a 10× objective and then delivered to a spectrometer (AvaSpec-2048L) for spectral recording with the spectral resolution of 0.2 nm. All optical measurements were carried out under ambient conditions and at room temperature.

3. Results and discussion

3.1. Silica nanoparticle film created by self-assembly

The dye-doped SNPs have high fluorescence and are well dispersed in an aqueous environment (Fig. 1a). Fluorescence from the SNPs is highly photostable as the dye molecules are encapsulated in the silica-based matrix, making it promising for biomarker. The average size of the SNPs is about 20 nm (Fig. 1b).

Dye-doped SNP films were obtained by self-assembly of the colloidal SNPs as shown in Fig. 1c. A 200 μL SNP suspension with a concentration of ~4.6×10^{14} particles/mL stored in a plastic microcentrifuge tube is heated at 70 °C for 3 h. Under the thermal effect, water evaporates which leads to fluid flows (carrying particles) from the centre to the edges where the contact line is pinned [14]. As a result, the film is self-assembly formed during the transition from wet to dry phase. After the evaporation process is complete, a thin layer of SNPs is obtained on the wall of the plastic microcentrifuge tube. For optical characterizations, the film is ground to small pieces, the so-called microslices. Fig. 1d presents the optical microscope image of fabricated microslices. Their size can vary from around 40 μm to 300 μm. Scanning electron microscope (SEM) image shows that the microslices have a relatively thin thickness (Fig. 1e). A high magnification SEM image of a sidewall of a typical microslice is shown in Fig. 1f indicating a thickness of around 2 μm.

3.2. Silica nanoparticles based random lasers in the air

The dye-doped SNP slices can work as efficient random microlasers under optical pumping. Fig. 2a shows the threshold behaviour, one of the most important signatures of lasing [15], from a SNP microslice with a quadrilateral shape and dimensions of around 130-150 μm. The PL intensity from the sample increases linearly with the pump pulse fluence until 16 mJ/cm^2 when the threshold is reached. Below the threshold, the emission is spontaneous which is characterized by a broad-spectrum and low intensity (top, left inset). Above the threshold, the emission intensity increases significantly and the spectrum becomes much narrower, indicating the evidence of stimulated emission (right, bottom inset). In particular, when the pump intensity increases only 2 times, from 9 to 18 mJ/cm^2, the PL intensity rises sharply, nearly 10 times, from 1340 to 12970 a. u. The threshold energy is comparable to random lasing in dye-doped silica nanopowders [12] but higher than that of other random lasing structures such as semiconductor powders [5] and photonic glasses [16].

Fig. 2b shows the narrowing of PL emission with increasing pump pulse fluence as another signature of lasing. The evolution of the full-width-at-half-maximum (FWHM) of the emission as a function of pump fluence is presented in Fig. 2c. Initially, FWHM of the PL emission is about 48 nm for fluence less than 4 mJ/cm^2. For higher fluences, the FWHM almost linearly decreases from 48 to 5.2 nm at 18 mJ/cm^2. At the threshold (15 mJ/cm^2), the FWHM is around 10 nm. For pump pulse fluences higher than 18 mJ/cm^2, the FWHM reaches its minimum of about 4 nm and maintains at this value for fluence up to 28 mJ/cm^2.

Studying the lasing mechanism is necessary to support lasing action. By a conventional definition, random lasing is stimulated radiation enables by optical amplification of light that undergoes multiple scattering [15]. In this work, we believe that the output emission is random lasing because the stimulated emission is amplified by multiple scattering. This claim is supported by the observation of optical modes on top of the stimulated emission background (Fig. 3). It is suggested that the sidewalls of the microslice can act as diffuse reflectors leading to light amplification via diffuse reflection. In other work, light is amplified by a Fabry–Perot-like cavity and the cavity length (L) is the distance between two sidewalls as shown in the inset of Fig. 3. Based on this idea, the free spectral range (FSR, the distance between two successive modes) of lasing modes can be estimated as FSR = $\lambda^2/(2nL)$, where

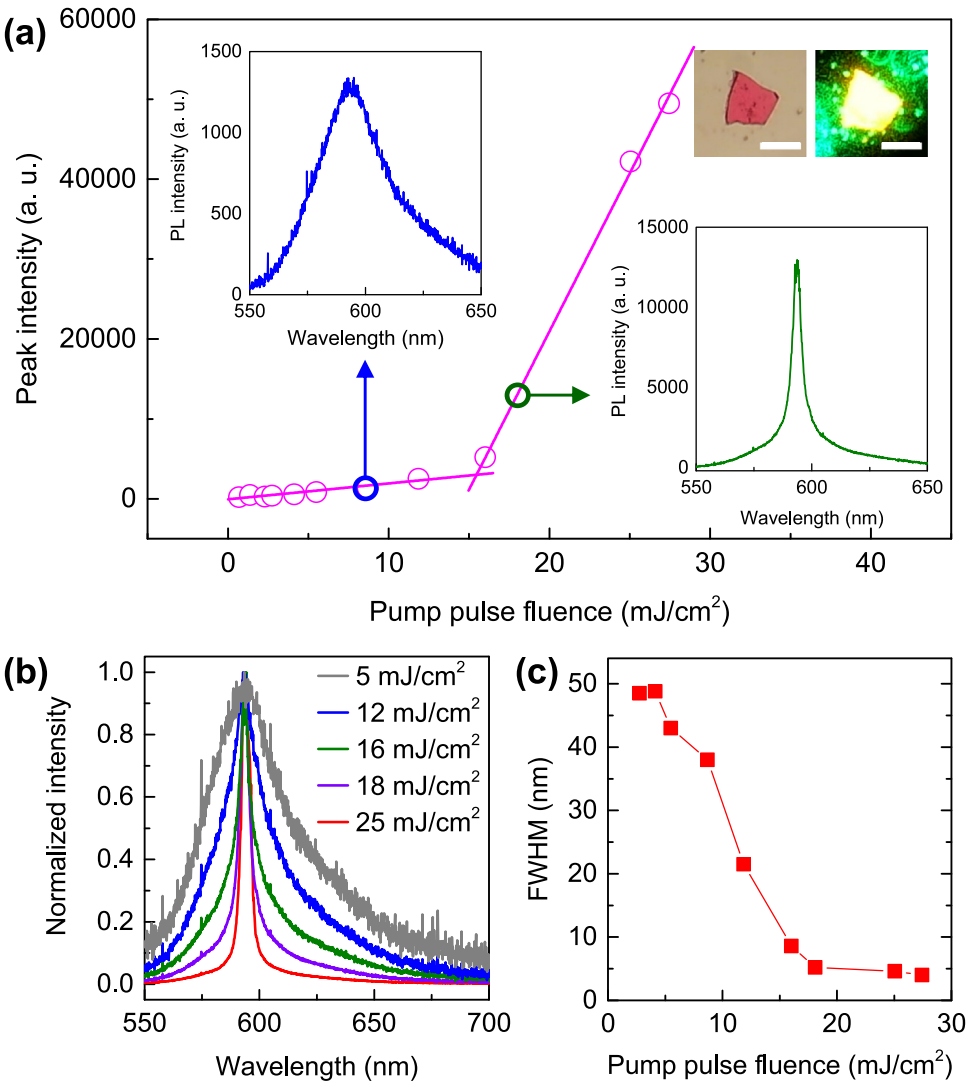

Fig. 2. (a) Peak intensity as a function of pump pulse fluence. Top left and bottom right insets show the PL spectrum below and above the lasing threshold, respectively. Top right insets present the optical and PL image of the sample. The scale bars are 200 μm. (b) Normalized PL intensity of emission spectra of the SNP microslice under various pump fluences. (c) Evolution of the FWHM of emission versus pump fluence.

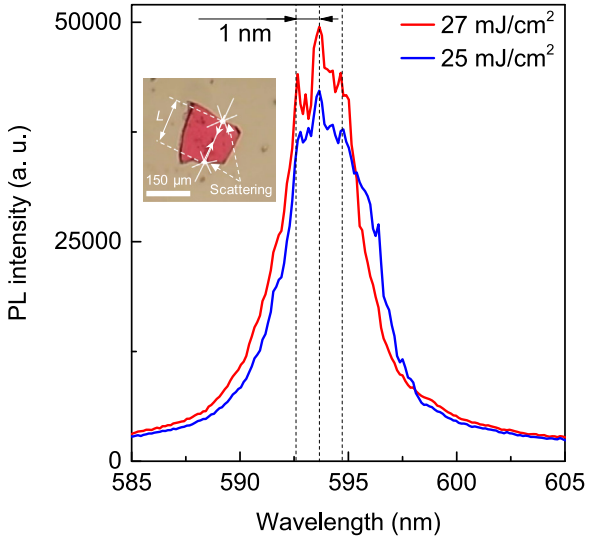

Fig. 3. Close-up emission spectrum of the microslice at the two highest pump fluences indicating the optical modes (denoted by dashed lines). The inset shows the proposed feedback mechanism for lasing action.

λ is the lasing wavelength, n is the refractive index of the microslice. From the emission spectrum, λ is determined to be 594 nm. From the microscope image, L is calculated to be 130 μm. Assuming $n = 1.46$ [17] then the calculated FSR is 0.93 nm, consistent with the experimental FSR of 1 nm (Fig. 3). This agreement supports the proposed mechanism for obtaining random lasing in the microslice structure. It expected that lasing modes can be more obvious if the scattering is stronger. This can be achieved by increasing the size of SNP as light scattering is strongly enhanced at Mie resonances. Indeed, it has been demonstrated recently that lasing emission can be obtained from a single microparticle due to strong Mie-resonant feedback [18].

3.3. Silica nanoparticles based random lasers in water

Random lasers with the ability to operate in an aqueous environment is an excellent candidate for a future generation biological sensing [19]. Fig. 4a shows emission spectrum from a SNP microslice immersed in water. The development from spontaneous emission at 15 mJ/cm^2 to stimulated (at 34 mJ/cm^2) and lasing emission at 73 mJ/cm^2 is distinctly observed. Peak intensity versus pump fluence is shown in Fig. 4b indicates the lasing threshold of around 41 mJ/cm^2. This value is nearly three times higher compared with that of the sample in the air. It is understandable because water has a higher refractive

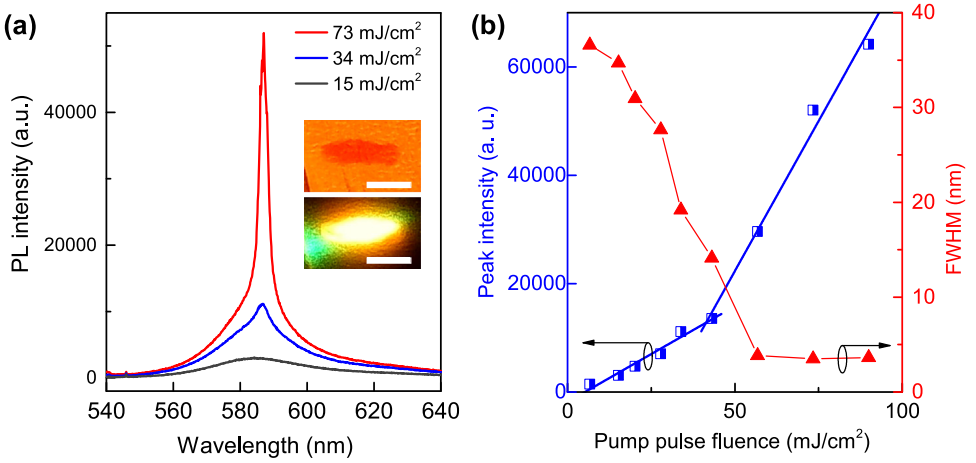

Fig. 4. (a) Emission spectra of a SNP microslice immersed in water. The insets present the optical and PL image of the corresponding sample. The scale bars are 200 μm. (b) Peak intensity and FWHM of emission spectra versus pump fluence.

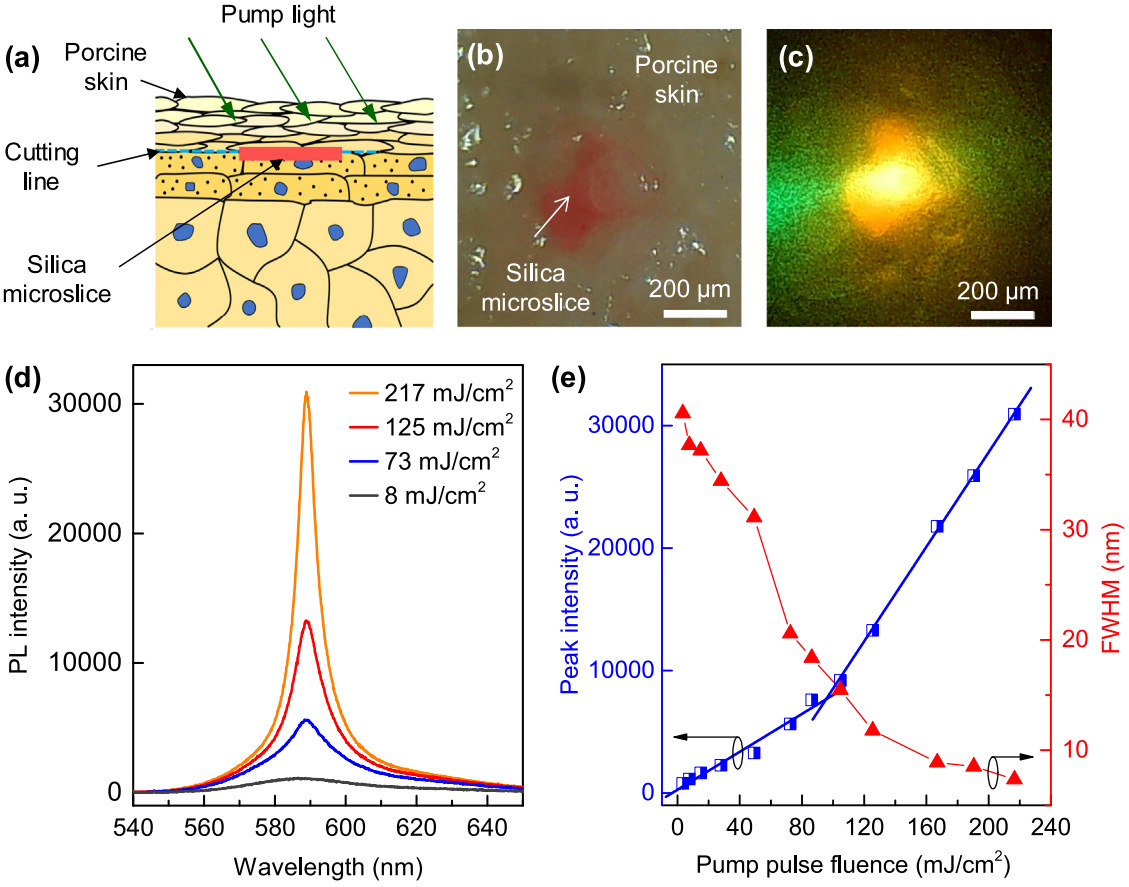

Fig. 5. (a) Schematic of random lasers implanted into the skin. (b) Optical microscope image of a laser embedded below the porcine skin surface. (c) PL image of the sample upon optical excitation. (d) Emission spectra of the embedded laser sample at various pump fluences. (e) Peak intensity and FWHM of emission spectra versus pump fluence.

index compared with air. Consequently, the optical confinement of the sample in water is lower due to the lower refractive index contrast and this leads to a higher threshold. In addition, it is noticeable that the lasing wavelength of the sample in water (around 587 nm) is 6 nm blue-shifted compared with that in the air. It is because the sample in water has lower optical confinement, and therefore, shorter wavelengths is less confined and easier to scatter out [20]. The evolution of FWHM of the emission versus pump fluence is similar to the laser sample in the air. The minimum FWHM measured is also around 4 nm.

3.4. Silica nanoparticles based random laser in the skin

Implantable lasers are significant for biological applications [21]. Recently, several kinds of conventional lasers such as microdroplet, microparticle, microdisk, nanowire have been successfully integrated into cell and tissue, providing a powerful tool to study cell migration, cancer invasion [22–26]. However, implantable random lasers have not been demonstrated. Herein, we show a proof-of-concept random laser capable of operating in the porcine skin tissue.

Pig skin was purchased from a local supplier and used directly. A razor was used to cut and open space just below the skin surface for inserting a microslice laser. After inserting, the laser is embedded into the skin as shown in Fig. 5a. The laser is still visible under an optical microscope because of the transparency of the thin skin layer (Fig. 5b). Upon optical excitation, a bright emission is observed from the laser sample (Fig. 5c). Their spectra indicate the evolution from spontaneous to stimulated emission with increasing pump fluence (Fig. 5d). The change of FWHM of the emission versus pump fluence is similar to that of laser sample in water but the lasing threshold, around 95 mJ/cm^2, is two times higher (Fig. 5e). It is because the skin is a strong light scattering medium thus only a portion of pumping energy passes through to excite the sample. Even though the lasing threshold is relatively high, the pumping energy is still far below the damage threshold of the skin [27] and may have a little effect on its structure and function. This achievement opens the possibility of utilizing random lasers for implanted biosensors and biological probes.

4. Conclusion

We have demonstrated fluorescent silica nanoparticles as an excellent candidate for random lasing. By using a simple and single-step fabrication process, dye-doped silica nanoparticles based random lasers can be obtained. The lasers have dimensions of around 100-200 μm and thickness of 2 μm. These lasers can operate in the air, water and porcine skin tissue under optical pulse excitation. The lasing properties in all conditions are similar excluding the lasing threshold which is the lowest in the air and highest in the porcine skin. Owing to the biocompatibility of silica, these lasers are safe for integrating into various biological environments such as blood and tissue, which is potential for bioimaging, biosensing and biological probes.

Declaration of competing interest

The authors declare that they have no known competing financial interests or personal relationships that could have appeared to influence the work reported in this paper.

Acknowledgement

This research is funded by the Vietnam's Ministry of Science and Technology under Project ĐTĐL.CN-40/19.

References

[1] F. Luan, B. Gu, A.S.L. Gomes, K.-T. Yong, S. Wen, P.N. Prasad, Lasing in nanocomposite random media, Nano Today 10 (2015) 168–192.
[2] D.S. Wiersma, The physics and applications of random lasers, Nat. Phys. 4 (2008) 359–367.
[3] B. Redding, M.A. Choma, H. Cao, Speckle-free laser imaging using random laser illumination, Nature Photon. 6 (2012) 355.
[4] N.M. Lawandy, R.M. Balachandran, A.S.L. Gomes, E. Sauvain, Laser action in strongly scattering media, Nature 368 (1994) 436–438.
[5] H. Cao, J.Y. Xu, E.W. Seelig, R.P.H. Chang, Microlaser made of disordered media, Appl. Phys. Lett. 76 (2000) 2997.
[6] S. Gottardo, R. Sapienza, P.D. García, A. Blanco, D.S. Wiersma, C. López, Resonance-driven random lasing, Nature Photon. 2 (2008) 429–432.
[7] Y. Wang, V.D. Ta, Y. Gao, T.C. He, R. Chen, E. Mutlugun, H.V. Demir, H.D. Sun, Stimulated emission and lasing from CdSe/CdS/ZnS Core-multi-shell quantum dots by simultaneous three-photon absorption, Adv. Mater. 26 (2014) 2954–2961.
[8] S. Santra, K. Wang, R. Tapec, W. Tan, Development of novel dye-doped silica nanoparticles for biomarker application, J. Biomed. Opt. 6 (2001) 160–166, 167.
[9] S.W. Bae, W. Tan, J.-I. Hong, Fluorescent dye-doped silica nanoparticles: new tools for bioapplications, Chem. Commun. 48 (2012) 2270–2282.
[10] H.N. Tran, T.H. Lien Nghiem, T.T. Duong Vu, M.T. Pham, T.V. Nguyen, T.T. Tran, V.H. Chu, K.T. Tong, T.T. Tran, T.T. Xuan Le, J.-C. Brochon, T.Q. Nguyen, M.N. Hoang, C.N. Duong, T.T. Nguyen, A.T. Hoang, P.H. Nguyen, Dye-doped silica-based nanoparticles for bioapplications, Adv. Nat. Sci-Nanosci. 4 (2013) 043001.
[11] S. Walia, A. Acharya, Silica micro/nanospheres for theranostics: from bimodal MRI and fluorescent imaging probes to cancer therapy, Beilstein J. Nanotechnol. 6 (2015) 546–558.
[12] S. García-Revilla, J. Fernández, M.A. Illarramendi, B. García-Ramiro, R. Balda, H. Cui, M. Zayat, D. Levy, Ultrafast random laser emission in a dye-doped silica gel powder, Opt. Express 16 (2008) 12251–12263.
[13] B. García-Ramiro, M.A. Illarramendi, S. García-Revilla, R. Balda, D. Levy, M. Zayat, J. Fernández, Lasing threshold of one- and two-photon-pumped dye-doped silica powder, Appl. Phys. B 117 (2014) 1135–1140.
[14] P.J. Yunker, T. Still, M.A. Lohr, A.G. Yodh, Suppression of the coffee-ring effect by shape-dependent capillary interactions, Nature 476 (2011) 308–311.
[15] R. Sapienza, Determining random lasing action, Nat. Rev. Phys. (2019).
[16] Y. Chen, J. Herrnsdorf, B. Guilhabert, Y. Zhang, A.L. Kanibolotsky, P.J. Skabara, E. Gu, N. Laurand, M.D. Dawson, Modification of emission wavelength in organic random lasers based on photonic glass, Org. Electron. 13 (2012) 1129–1135.
[17] N. Suzuki, Y. Tomita, Silica-nanoparticle-dispersed methacrylate photopolymers with net diffraction efficiency near 100%, Appl. Opt. 43 (2004) 2125–2129.
[18] E. Tiguntseva, K. Koshelev, A. Furasova, V. Mikhailovskii, E. Ushakova, D. Baranov, T. Shegai, A. Zakhidov, Y. Kivshar, S. Makarov, Single-particle Mie-resonant all-dielectric nanolasers, arXiv:1905.086462019.
[19] S. Caixeiro, M. Gaio, B. Marelli, F.G. Omenetto, R. Sapienza, Silk-based biocompatible random lasing, Adv. Opt. Mater. 4 (2016) 998–1003.
[20] S. Tang, R. Derda, Q. Quan, M. Loncar, G.M. Whitesides, Continuously tunable microdroplet-laser in a microfluidic channel, Opt. Express 19 (2011) 2204–2215.
[21] Y.-C. Chen, X. Fan, Biological lasers for biomedical applications, Adv. Opt. Mater. 7 (2019) 1900377.
[22] M. Humar, S. Hyun Yun, Intracellular microlasers, Nature Photon. 9 (2015) 572–576.
[23] M. Humar, A. Dobravec, X. Zhao, S.H. Yun, Biomaterial microlasers implantable in the cornea, skin, and blood, Optica 4 (2017) 1080–1085.
[24] A.H. Fikouras, M. Schubert, M. Karl, J.D. Kumar, S.J. Powis, A. Di Falco, M.C. Gather, Non-obstructive intracellular nanolasers, Nature Commun. 9 (2018) 4817.
[25] N. Martino, S.J.J. Kwok, A.C. Liapis, S. Forward, H. Jang, H.-M. Kim, S.J. Wu, J. Wu, P.H. Dannenberg, S.-J. Jang, Y.-H. Lee, S.-H. Yun, Wavelength-encoded laser particles for massively multiplexed cell tagging, Nature Photon. 13 (2019) 720–727.
[26] E.I. Galanzha, R. Weingold, D.A. Nedosekin, M. Sarimollaoglu, J. Nolan, W. Harrington, A.S. Kuchyanov, R.G. Parkhomenko, F. Watanabe, Z. Nima, A.S. Biris, A.I. Plekhanov, M.I. Stockman, V.P. Zharov, Spaser as a biological probe, Nature Commun. 8 (2017) 15528.
[27] R. Vincelette, G. Noojin, C. Harbert, K. Schuster, A. Shingledecker, D. Stolarski, S. Kumru, J. Oliver, Porcine skin damage thresholds for 0.6 to 9.5 cm beam diameters from 1070-nm continuous-wave infrared laser radiation, J. Biomed. Opt. 19 (2014) 035007.